V European Conference on Computational Fluid Dynamics
ECCOMAS CFD 2010
J. C. F. Pereira and A. Sequeira (Eds)
Lisbon, Portugal,14-17 June 2010

# HEMODYNAMICS AT THE MESOSCALE: A COARSE-GRAINED LATTICE BOLTZMANN-MOLECULAR DYNAMICS APPROACH

**Florian Janoschek, Jens Harting, and Federico Toschi**

Eindhoven University of Technology, Department of Applied Physics
P. O. Box 513, 5600 MB Eindhoven, The Netherlands
e-mail: {fjanoschek,j.harting,f.toschi}@tue.nl

**Key words:** Blood rheology, Coarse grained hemodynamics, Lattice Boltzmann simulation, Soft particle suspensions

**Abstract.** *Simulation of human blood flow is a demanding task both in terms of the complexity of applicable models and the computational effort. One reason is the particulate nature of blood which in first approximation may be treated as a suspension of red blood cells (RBCs) in blood plasma.*

*A second reason is that in realistic geometries typical length scales vary over several orders of magnitude. Usual computational models either cope with this complexity by implementing only a homogenous although non-Newtonian fluid or highly resolve relatively small numbers of RBCs by means of deformable meshes.*

*We developed a coarse-grained and highly efficient yet still particulate model for blood that allows us to simulate up to millions of cells on current parallel supercomputers. We start with a lattice Boltzmann based method for the simulation of suspensions of rigid particles which accounts for long-range hydrodynamic interactions. Real RBCs, however, are not rigid. We thus add anisotropic model potentials to cover the more complex short-range behavior of deformable cells on a phenomenological level. In this work, we study the effect of the model parameters and demonstrate the applicability of the model to simple situations of confined flow as well as its scalability.*

## 1 INTRODUCTION

Human blood can be approximated as a suspension of deformable red blood cells (RBCs, also called erythrocytes) in a Newtonian liquid, the blood plasma. The other constituents like leukocytes and thrombocytes can be neglected due to their low volume concentrations[1]. Typical concentrations for RBCs are 40 to 50 % under physiological conditions. In the absence of external stresses, erythrocytes assume the shape of biconcave discs of approximately 8 $\mu$m diameter[2]. An understanding of their effect on the rheology and the clotting behavior of blood is necessary for the study of pathological deviations in the body and the design of microfluidic devices for improved blood analysis.

Well-established methods for the computer simulation of blood flow either consist of an elaborate model of deformable cells[3,4] or restrict themselves to a continuous description at larger scales[5]. Our motivation is to bridge the gap between both classes of models by an intermediate approach: we keep the particulate nature of blood, but simplify the description of each cell as far as possible[6]. The ultimate goal is to perform large-scale simulations that allow to study the flow in realistic geometries but also to link bulk properties, for example the effective viscosity, to phenomena at the level of single erythrocytes. Only a computationally efficient description allows the reliable accumulation of statistical properties in time-dependent flows which is necessary for this task. The improved understanding of the dynamic behavior of blood might be used for the optimization of macroscopic simulation methods.

The main idea of our model is to distinguish between the long-range hydrodynamic coupling of cells and the short-range interactions that are related to the complex mechanics, electrostatics, and the chemistry of the membranes. The short-range behavior of RBCs is described on a phenomenological level by means of anisotropic model potentials. Long-range hydrodynamic interactions are accounted for by means of a lattice Boltzmann (LB) method[7]. Our model is well suited for the implementation of complex boundary conditions and an efficient parallelization on parallel supercomputers. Both are necessary for the study of realistic systems like branching vessels and the accumulation of statistically relevant data in bulk flow situations. Various authors already applied the LB method to blood flow at a large variety of scales[5,4]. Since we are interested in a minimal resolution of RBCs we decide for a method for suspensions of rigid discs of finite size. However, in contrast to other works[8] our implementation allows the particles to overlap in order to take into account the deformability of the erythrocytes.

## 2 HYDRODYNAMIC PART OF THE MODEL

We apply a D3Q19/BGK LB method for modeling the blood plasma[9]. See the book of Succi for a comprehensive introduction[7]. The single particle distribution function $n_r(\mathbf{x}, t)$ resembles the fluid traveling with one of $r = 1, \ldots, 19$ discrete velocities $\mathbf{c}_r$ at the three-dimensional lattice position $\mathbf{x}$ and discrete time $t$. Its evolution in time is determined by

the lattice Boltzmann equation

$$n_r(\mathbf{x}+\mathbf{c}_r,t+1) = n_r(\mathbf{x},t) - \Omega \ , \quad \text{with} \quad \Omega = \frac{n_r(\mathbf{x},t) - n_r^{\mathrm{eq}}(\rho(\mathbf{x},t),\mathbf{u}(\mathbf{x},t))}{\tau} \tag{1}$$

being the BGK-collision term with a single relaxation time $\tau$. The equilibrium distribution function $n_r^{\mathrm{eq}}(\rho,\mathbf{u})$ is an expansion of the Maxwell-Boltzmann distribution. $\rho(\mathbf{x},t) = \sum_r n_r(\mathbf{x},t)$ and $\rho(\mathbf{x},t)\mathbf{u}(\mathbf{x},t) = \sum_r n_r(\mathbf{x},t)\mathbf{c}_r$ can be identified as density and momentum. In the limit of small velocities and lattice spacings the Navier-Stokes equations are recovered with a kinematic viscosity of $\nu = (2\tau-1)/6$, where $\tau = 1$ in this study.

For a coarse-grained description of the hydrodynamic interaction of cells and blood plasma, a method similar to the one by Aidun et al. modeling rigid particles of finite size is applied[10,8]. Starting point is the mid-link bounce-back boundary condition: the confining geometry is discretized on the lattice and all accordant nodes are turned into fluid-less wall nodes. If $\mathbf{x}$ is such a node the updated distribution at $\mathbf{x}+\mathbf{c}_r$ is determined as

$$n_r(\mathbf{x}+\mathbf{c}_r,t+1) = n_{\bar{r}}^*(\mathbf{x}+\mathbf{c}_r,t) \ , \quad \text{with} \quad n_r^*(\mathbf{x},t) = n_r(\mathbf{x},t) - \Omega \ . \tag{2}$$

This corresponds to replacing the local distribution in direction $r$ with the post-collision distribution $n_r^*(\mathbf{x},t)$ of the opposite direction $\bar{r}$. To model boundaries moving with velocity $\mathbf{v}$, Eq. 2 needs to be modified. The new update rule

$$n_r(\mathbf{x}+\mathbf{c}_r,t+1) = n_{\bar{r}}^*(\mathbf{x}+\mathbf{c}_r,t) + C \ , \quad \text{with} \quad C = \frac{2\alpha_{c_r}}{c_{\mathrm{s}}^2}\rho(\mathbf{x}+\mathbf{c}_r,t)\,\mathbf{c}_r\mathbf{v} \tag{3}$$

was chosen consistently with $n_r^{\mathrm{eq}}(\rho,\mathbf{u})$ for the general case $\mathbf{u} = \mathbf{v} \neq \mathbf{0}$. The lattice weights $\alpha_{c_r}$ and the speed of sound $c_{\mathrm{s}}$ are constants for a given set of discrete velocities. The momentum

$$\Delta\mathbf{p}_{\mathrm{fp}} = (2n_{\bar{r}} + C)\,\mathbf{c}_{\bar{r}} \ , \tag{4}$$

which is transferred during each time step by each single bounce-back process is used to calculate the resulting force on the boundary. When a freely moving particle is modeled by this method its discretization on the lattice needs to be updated occasionally. During this process, fluid nodes are created or vanish and the related change in total fluid momentum is balanced by an additional force on the respective particle.

Instead of the biconcave equilibrium shape of physiological RBCs we choose a simplified ellipsoidal geometry that is defined by two distinct half-axes $R_\parallel$ and $R_\perp$ parallel and perpendicular to the unit vector $\hat{\mathbf{o}}_i$ which points along the direction of the axis of rotational symmetry of each particle $i$. Since the cell-fluid interaction volumes are rigid we need to allow them to overlap in order to account for the deformability of real erythrocytes. We thus assume a pair of mutual forces

$$\mathbf{F}_{\mathrm{pp}}^{+} = 2n_r^{\mathrm{eq}}(\bar{\rho},\mathbf{u}=\mathbf{0})\mathbf{c}_r \qquad \text{and} \qquad \mathbf{F}_{\mathrm{pp}}^{-} = 2n_{\bar{r}}^{\mathrm{eq}}(\bar{\rho},\mathbf{u}=\mathbf{0})\mathbf{c}_{\bar{r}} = -\mathbf{F}_{\mathrm{pp}}^{+} \tag{5}$$

at each cell-cell link. This is exactly the momentum transfer during one time step due to the rigid-particle algorithm for a resting particle and an adjacent site with resting fluid at equilibrium and initial density $\bar{\rho}$. In case of close contact of cells with the confining geometry we proceed in a similar manner as for two cells but ignore forces on the system walls.

## 3 MODEL POTENTIALS

In order to account for the complex behavior of real RBCs at small distances we add phenomenological pair potentials. As a simple way to describe elastic deformability, we use the repulsive branch of a Hookian spring potential

$$\phi(r_{ij}) = \begin{cases} \varepsilon \left(1 - r_{ij}/\sigma\right)^2 & r_{ij} < \sigma \\ 0 & r_{ij} \geq \sigma \end{cases} \tag{6}$$

for the scalar displacement $r_{ij}$ of two cells $i$ and $j$. With respect to the disc-shape of RBCs, we follow the approach of Berne and Pechukas[11] and choose the energy and range parameters

$$\varepsilon(\hat{\mathbf{o}}_i, \hat{\mathbf{o}}_j) = \frac{\bar{\varepsilon}}{\sqrt{1 - \chi^2 \left(\hat{\mathbf{o}}_i \hat{\mathbf{o}}_j\right)^2}} \,, \quad \sigma(\hat{\mathbf{o}}_i, \hat{\mathbf{o}}_j, \hat{\mathbf{r}}_{ij}) = \frac{\bar{\sigma}}{\sqrt{1 - \frac{\chi}{2}\left[\frac{(\hat{\mathbf{r}}_{ij}\hat{\mathbf{o}}_i + \hat{\mathbf{r}}_{ij}\hat{\mathbf{o}}_j)^2}{1+\chi\hat{\mathbf{o}}_i\hat{\mathbf{o}}_j} + \frac{(\hat{\mathbf{r}}_{ij}\hat{\mathbf{o}}_i - \hat{\mathbf{r}}_{ij}\hat{\mathbf{o}}_j)^2}{1-\chi\hat{\mathbf{o}}_i\hat{\mathbf{o}}_j}\right]}} \tag{7}$$

as functions of the orientations $\hat{\mathbf{o}}_i$ and $\hat{\mathbf{o}}_j$ of the cells and their normalized center displacement $\hat{\mathbf{r}}_{ij}$. We achieve an anisotropic potential with a zero-energy surface that is approximately that of ellipsoidal discs. Their half-axes parallel $\sigma_\parallel$ and perpendicular $\sigma_\perp$ to the symmetry axis enter Eq. 7 via $\bar{\sigma} = 2\sigma_\perp$ and $\chi = (\sigma_\parallel^2 - \sigma_\perp^2)/(\sigma_\parallel^2 + \sigma_\perp^2)$ whereas $\bar{\varepsilon}$ determines the potential strength. For modeling the cell-wall interaction we assume a sphere with radius $\sigma_\mathrm{w} = 1/2$ at every lattice node on the surface of a vessel wall and implement similar forces as for the cell-cell interaction. Using

$$\sigma(\hat{\mathbf{o}}_i, \hat{\mathbf{r}}_{i\mathbf{x}}) = \frac{\bar{\sigma}_\mathrm{w}}{\sqrt{1 - \chi_\mathrm{w} \left(\hat{\mathbf{r}}_{i\mathbf{x}}\hat{\mathbf{o}}_i\right)^2}} \tag{8}$$

as a range parameter with $\bar{\sigma}_\mathrm{w} = \sqrt{\sigma_\perp^2 + \sigma_\mathrm{w}^2}$ and $\chi_\mathrm{w} = (\sigma_\parallel^2 - \sigma_\perp^2)/(\sigma_\parallel^2 + \sigma_\mathrm{w}^2)$ allows to scale a potential with radial symmetry to fit for the description of the interaction of a sphere and an ellipsoidal disc[11]. The parameter $\varepsilon(\hat{\mathbf{o}}_i, \hat{\mathbf{o}}_j) = \bar{\varepsilon}_\mathrm{w}$ remains constant in this case. $\hat{\mathbf{r}}_{i\mathbf{x}}$ is the normalized center displacement of cell $i$ and a wall node $\mathbf{x}$.

Fig. 1 shows an outline of the full model. For two RBCs the inner volume implementing the cell-plasma interaction with half axes $R_\parallel$ and $R_\perp$ is shown. Also depicted are the larger volumes that are defined by the range parameters $\sigma_\parallel$ and $\sigma_\perp$ of the cell-cell and cell-wall interaction. A section of a vessel wall is visualized by means of spheres with radius $\sigma_\mathrm{w}$ according to the cell-wall potential. The forces emerging from the interaction of the

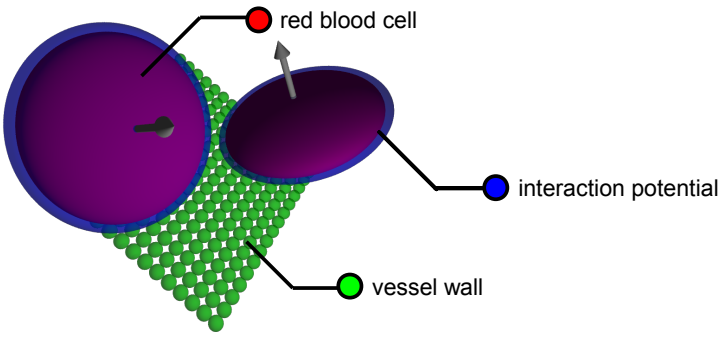


Figure 1: Outline of the model. Shown are two cells with their axes of rotational symmetry depicted by vectors. The volumes defined by the cell-cell interaction are approximately ellipsoidal. The smaller ellipsoidal volumes of the cell-plasma interaction are discretized on the underlying lattice. The cell-wall potential assumes spheres with radius $\sigma_\mathrm{w}$ on all surface wall nodes.

cells with the fluid, other RBCs, and walls are integrated by a classical MD code in order to evolve the system in time. Both LB and MD routines use the same domain decomposition. For more detailed information concerning the model we refer to the upcoming publication[6].

## 4 RESULTS

All quantities can be converted from simulation units to physical units by multiplication with products of integer powers of the conversion factors $\delta x$, $\delta t$, and $\delta m$ for space, time, and mass. As a convention in this work, primed variables are used to distinguish quantities given in physical units from the same unprimed variable measured in lattice units. We choose one lattice spacing to be $\delta x = 2/3\,\mu\mathrm{m}$ which ensures that RBCs are discretized as contiguous and closed volumes. Supposing that $\nu$ matches the kinematic plasma viscosity of $\nu' = 1.09 \times 10^{-6}\,\mathrm{m}^2/\mathrm{s}$ determines the time discretization as $\delta t = 6.80 \times 10^{-8}\,\mathrm{s}$. $\delta m = 3.05 \times 10^{-16}\,\mathrm{kg}$ is chosen arbitrarily. We investigate the influence of the different model parameters on the effective dynamic viscosity $\mu_\mathrm{eff}$ for a homogenous suspension of cells in plane Couette flow as a function of the shear rate. All simulations reported here are performed on a system with a size of $n_x = 128$ lattice units in $x$- and $n_y = n_z = 40$ lattice units in $y$- and $z$-direction or $85 \times 27^2\,\mu\mathrm{m}^3$ of real blood. Between the two $yz$-side planes a constant offset of the local fluid velocities in $z$-direction is imposed by an adaption of the Lees-Edwards shear boundary condition to the LB method[12].

First the influence of the volume of the cell-fluid interaction is studied. Fig. 2(a) shows the viscosity as a function of the shear rate for different $R_\parallel$ and $R_\perp$ at a cell number concentration that varies by less than 5 %. Generally, shear thinning is visible, but both the absolute viscosities and the change in viscosity per shear rate increase significantly for larger interaction volumes. Based on this result and the experiences from additional parameter studies we choose the largest investigated value of $R'_\perp = 11/3\,\mu\mathrm{m}$ but with respect to Fig. 2(a) modify the aspect ratio to $R_\perp = 3R_\parallel$. We now define

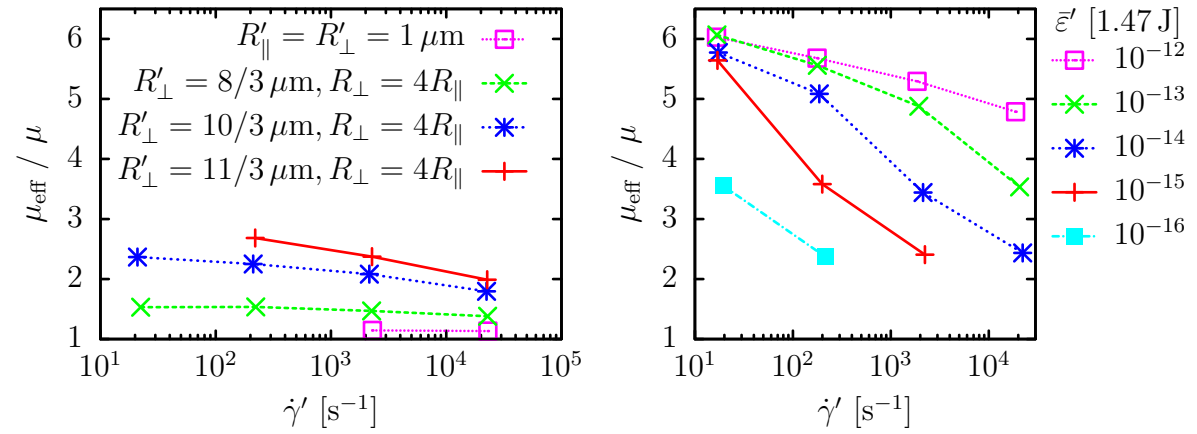


(a) (b)

Figure 2: Effective viscosity $\mu_{\text{eff}}$ in dependence on the shear rate $\dot{\gamma}$ as calculated for Couette flow for different sets of model parameters. In (a), $\sigma'_\perp = 4\,\mu$m, $\sigma'_\parallel = 1\,\mu$m, and $\bar{\varepsilon}' = 1.47\times10^{-14}$ J is kept fixed and the volume implementing the cell-fluid interaction is varied by means of $R_\parallel$ and $R_\perp$. The cell-fluid volume concentration varies within 2.6 % and 36 %. Larger volumes $4\pi R_\perp^2 R_\parallel/3$ lead to more pronounced shear thinning and generally higher viscosities. In (b), $\sigma'_\perp = 4\,\mu$m, $\sigma'_\parallel = 4/3\,\mu$m, and $R_\perp/\sigma_\perp = R_\parallel/\sigma_\parallel = 11/12$ is kept constant and the strength parameter $\bar{\varepsilon}$ of the cell-cell interaction is varied at a cell-fluid volume concentration of 43 %. Increasing $\bar{\varepsilon}$ seemingly leads to a shift of the curve to higher shear rates $\dot{\gamma}$ while the viscosity for a given shear rate generally becomes larger yet more stable.

$R_\perp/\sigma_\perp = R_\parallel/\sigma_\parallel = 11/12$ and achieve values for the cell-cell interaction diameters $2\sigma'_\parallel$ and $2\sigma'_\perp$ and the associated volume $4\pi\sigma'_\parallel{\sigma'_\perp}^2/3$ that closely resemble the respective values of physiological erythrocytes[2].

In further simulations the effect of the stiffness parameter of the cell-cell potential $\bar{\varepsilon}$ is studied. The viscosity as a function of the shear rate as plotted in Fig. 2(b) shows that generally the viscosity increases with increasing $\bar{\varepsilon}$. For very stiff cells the dependence on the shear rate decreases considerably. This is in asymptotic consistency with the experimental results of Chien[13] who measured the effective viscosity of a suspension of artificially hardened RBCs and found a significantly increased yet mostly constant viscosity. The cell-fluid volume concentration of 43 % in Fig. 2(b) seems sufficiently close to the hematocrit of 45 % in the measurements done by Chien[13] to justify a quantitative comparison. We find best agreement for $\bar{\varepsilon}' = 1.47 \times 10^{-15}$ J and use this parametrization for the following investigations.

To demonstrate the effect of confinement on our model we study steady flow through a cylindrical channel with a radius of 31 $\mu$m and a length of 43 $\mu$m with periodic boundaries. The cell-fluid volume concentration is now 42 %. We choose $\bar{\varepsilon}'_{\text{w}} = 1.47 \times 10^{-16}$ J for the strength of the cell-wall interaction. Fig. 3(a) visualizes the cells as the volumes defined by the cell-cell interaction and the channel wall as midplane between fluid and wall nodes. A strong alignment of the cells with shear is present. In Fig. 3(b), the normalized radial

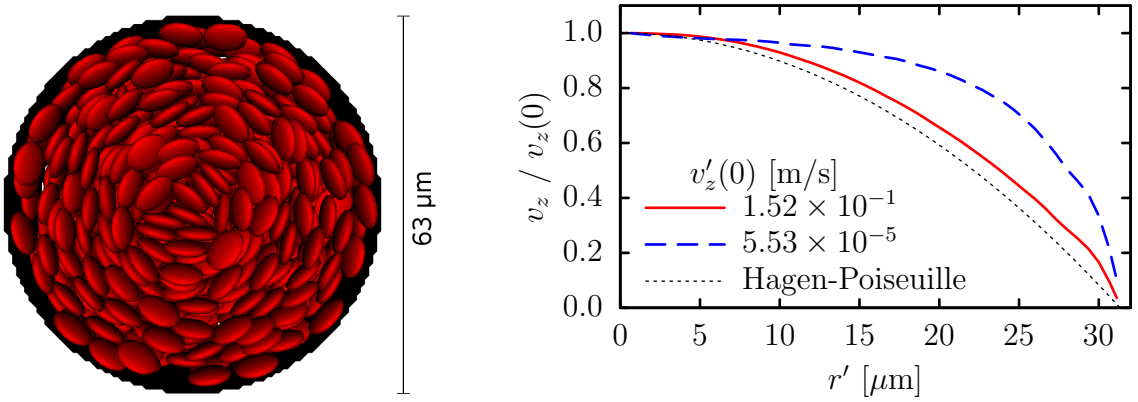


(a) (b)

Figure 3: Steady flow through a cylindrical channel with a radius of 31 $\mu$m at 42 % cell-fluid volume concentration. In (a), the volumes defined by the cell-cell interaction and the midplane between wall and fluid nodes are displayed. The flow is pointing into the drawing plane and has a maximum velocity of $1.08 \times 10^{-2}$ m/s at the center. Layering of the cells in shear flow can be observed. (b) shows the radial velocity profile for two different flow rates. Each curve is normalized to the respective maximum velocity at the center. The parabolic Hagen-Poiseuille profile is plotted as well for comparison. Apparent slip due to a cell depletion layer is visible. The blunting at low flow rates is in qualitative agreement with literature data[1].

velocity profiles for two flow velocities are compared. Close to the wall, apparent slip is visible. It is due to a cell depletion layer and to some extent can be controlled via $\bar{\varepsilon}_\mathrm{w}$. While for the highest velocity the curve looks parabolic in the central region, there are geometrically induced ordering effects and increasing blunting when the flow rate is reduced. The blunting is qualitatively consistent with experimental data from the literature[1]. Also the presence of cell alignment in shear flow is well known. The same holds for a cell depletion layer close to vessel walls[14].

In the following study of the flow of nine RBCs through branching capillaries with a radius of 4.7 $\mu$m particulate effects play an even more important role. One of the branches features a stenosis with only 2.7 $\mu$m radius. Both tube diameters and Reynolds numbers $Re \lesssim 4 \times 10^{-3}$ match physiological situations[14]. We vary the cell-wall interaction stiffness $\bar{\varepsilon}_\mathrm{w}$ and find that the constricted branch gets clogged for $\bar{\varepsilon}'_\mathrm{w} = 1.47 \times 10^{-15}$ J. This can be seen from the RBC trajectories displayed in Fig. 4(a) together with a cut through the geometry and from the development of the relative flow rate in the respective branch over time in Fig. 4(b). For $\bar{\varepsilon}'_\mathrm{w} = 1.47 \times 10^{-17}$ J, however, the erythrocytes easily pass the constriction as expected for healthy cells[1] and the flow rate does not change except for fluctuations induced by the mutable configuration of RBCs in the system. In the case of an intermediate value of $\bar{\varepsilon}'_\mathrm{w} = 1.47 \times 10^{-16}$ J, cells are initially stopped but due to pressure fluctuations get squeezed through the stenosis eventually. The acceleration by the cell-wall potential when leaving the constriction leads to the peaks of the flow rate visible in Fig. 4(b).

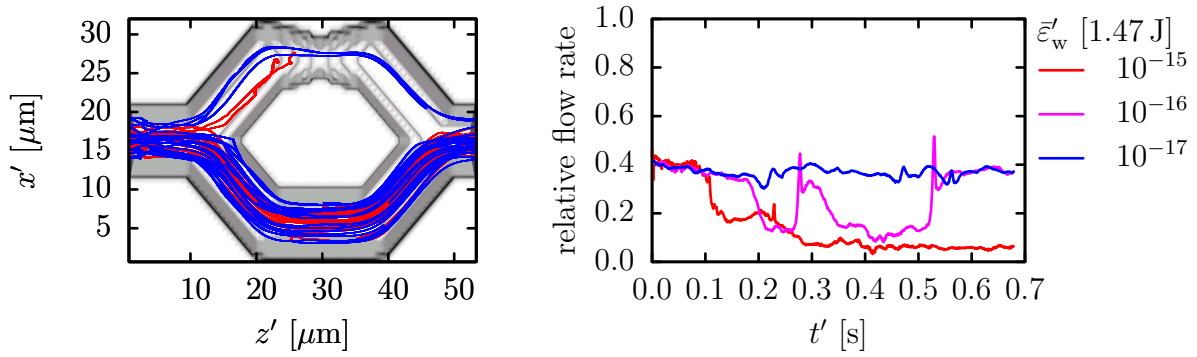


(a) (b)

Figure 4: Flow through a branching capillary. The channel radius is $R'_{\mathrm{s}} = 2.7\,\mu$m at a stenosis in the upper branch and $4.7\,\mu$m otherwise. (a) compares the center trajectories of nine cells for a cell-wall interaction stiffness of either $\bar{\varepsilon}'_{\mathrm{w}} = 1.47 \times 10^{-15}$ J or $\bar{\varepsilon}'_{\mathrm{w}} = 1.47 \times 10^{-17}$ J. Also visualized is a cut of the midplane between wall and fluid nodes. The flow direction is pointing from left to right. (b) depicts the time evolution of the relative volume flow rate through the constricted branch for different values of $\bar{\varepsilon}'_{\mathrm{w}}$. The clogging in the case of $\bar{\varepsilon}'_{\mathrm{w}} = 1.47 \times 10^{-15}$ J becomes visible both in the trajectories and in a drop of the relative flow rate to less than 10 %. While $\bar{\varepsilon}'_{\mathrm{w}} = 1.47 \times 10^{-17}$ J leads to a continuous flow situation, there are temporary drops and sharp peaks of the flow rate for $\bar{\varepsilon}'_{\mathrm{w}} = 1.47 \times 10^{-16}$ J. They can be explained by RBCs being initially stopped at the stenosis and eventually squeezed through due to local pressure fluctuations.

While the results for the larger channel studied above could still mostly be reproduced by a homogenous fluid with a specially tuned shear-rate dependent viscosity $\mu(\dot{\gamma})$, this is not possible at the scale of capillaries. Our model allows to account for clearly particulate effects like clogging or local changes of flow rate and pressure. In Fig. 4(a), the interplay of both of them prevents further cells from entering the constricted branch after its closure as expected from the literature[14].

Despite the simplifications of the model, parallel supercomputers are necessary to simulate more realistic vessel networks or large bulk systems. This makes the scalability of the code crucial. For a quasi-homogenous chunk of suspension consisting of $1024^2 \times 2048$ lattice sites and $4.1 \times 10^6$ cells (see Fig. 5(a)) simulated on a BlueGene/P system, we achieve a parallel efficiency normalized to the case of 2048-fold parallelism of 95.7 % on 16384 and still 85.2 % on 32768 cores. In comparison, the pure LB code without the MD routines shows a relative parallel efficiency of 98.1 % on 32768 cores. The parallel performance of the combined code is mainly limited by the relation of the interaction range of a cell to the size of the computational domain dedicated to each task. The full strong scaling behavior for 1024 to 32768 cores is shown in Fig. 5(b). Compared to deformable particle models[4], our method not only has a lower overall number of computations at a given resolution but is also easier to parallelize efficiently because each RBC has only six degrees of freedom.

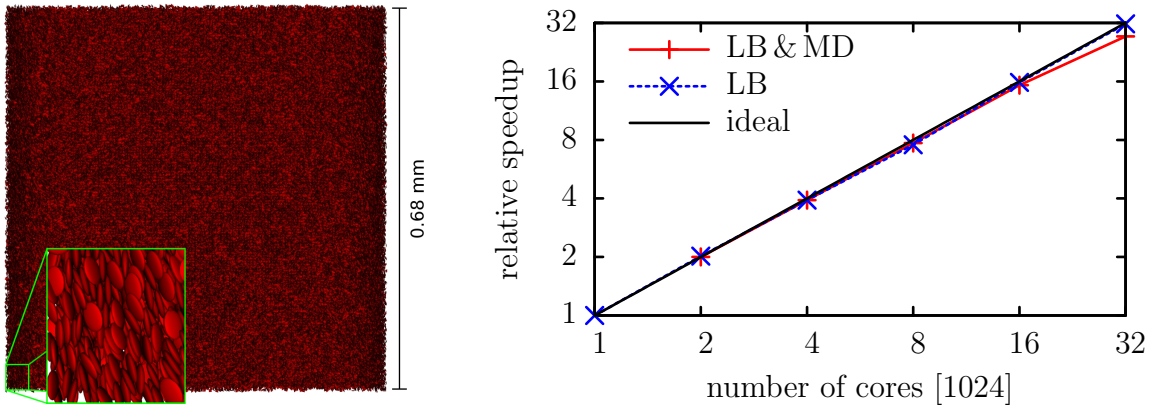


(a) (b)

Figure 5: Strong scaling benchmark on the BlueGene/P system at JSC. (a) shows the benchmark system consisting of $4.1 \times 10^6$ cells and $1024^2 \times 2048$ lattice sites which resembles $0.68^2 \times 1.37\,\mathrm{mm}^3$ of blood. In (b) the relative speedup is plotted as a function of the number of cores for the full model (LB & MD) and a cell-free fluid volume of the same size (LB).

## 5 CONCLUSION

The results presented above suggest that our model bears the potential to reproduce the particulate behavior of blood on a large range of spatial scales. Clearly, our motivation is not to replace models with higher resolution like the one presented by Dupin et al.[4], but instead to tune our model to reproduce their results as well as experimental data and bridge the gap to scales that are inaccessible for higher resolution methods. For this task, the reproduction of effects related to simple confined flows is a proper way to calibrate and validate the model. We are confident that our new method will prove both an efficient tool for coarse grained yet particulate simulations of flow in complex geometries and a valuable contribution to the improvement of macroscopic blood modeling.

## 6 ACKNOWLEDGMENTS

The authors thank A. C. B. Bogaerds and F. N. v. d. Vosse for fruitful discussions and S. Plimpton for providing his freely available MD code *ljs*[15]. Financial support is gratefully acknowledged from the Landesstiftung Baden-Württemberg, the HPC-Europa2 project, the DEISA2 project, the collaborative research centre (SFB) 716, and the TU/e High Potential Research Program. Further, the authors acknowledge computing resources from JSC Jülich, SSC Karlsruhe, and SARA Amsterdam.

## References

[1] H. L. Goldsmith and R. Skalak. Hemodynamics. *Annu. Rev. Fluid Mech.*, 7:213–247, 1975.

[2] E. Evans and Y. C. Fung. Improved measurements of the erythrocyte geometry. *Microvascular Research*, 4:335–347, 1972.

[3] H. Noguchi and G. Gompper. Shape transitions of fluid vesicles and red blood cells in capillary flows. *PNAS*, 102(40):14159–14164, 2005.

[4] M. M. Dupin, I. Halliday, C. M. Care, L. Alboul, and L. L. Munn. Modeling the flow of dense suspensions of deformable particles in three dimensions. *Phys. Rev. E*, 75: 066707, 2007.

[5] J. Boyd, J. M. Buick, and S. Green. Analysis of the Casson and Carreau-Yasuda non-Newtonian blood models in steady and oscillatory flows using the lattice Boltzmann method. *Phys. Fluids*, 19:093103, 2007.

[6] F. Janoschek and J. Harting. A simplified particulate model for coarse-grained hemodynamics simulations. In preparation, 2010.

[7] S. Succi. *The Lattice Boltzmann Equation for Fluid Dynamics and Beyond*. Numerical Mathematics and Scientific Computation. Oxford University Press, 2001.

[8] N.-Q. Nguyen and A. J. C. Ladd. Lubrication corrections for lattice-Boltzmann simulations of particle suspensions. *Phys. Rev. E*, 66:046708, 2002.

[9] Y. H. Qian, D. d'Humières, and P. Lallemand. Lattice BGK models for Navier-Stokes equation. *Europhys. Lett.*, 17(6):479–484, February 1992.

[10] C. K. Aidun, Y. Lu, and E.-J. Ding. Direct analysis of particulate suspensions with inertia using the discrete Boltzmann equation. *J. Fluid Mech.*, 373:287–311, 1998.

[11] B. J. Berne and P. Pechukas. Gaussian model potentials for molecular interactions. *J. Chem. Phys.*, 56(8):4213–4216, April 1972.

[12] A. J. Wagner and J. M. Yeomans. Phase separation under shear in two-dimensional binary fluids. *Phys. Rev. E*, 59(4):4366–4373, 1999.

[13] S. Chien. Shear dependence of effective cell volume as a determinant of blood viscosity. *Science*, 168(3934):977–979, 1970.

[14] Y. C. Fung. *Biomechanics. Mechanical Properties of Living Tissues*. Springer, New York, 1981.

[15] S. Plimpton. Fast parallel algorithms for short-range molecular dynamics. *J. Comp. Phys.*, 117:1–19, 1995.